Al-Qadisiyah Journal of Pure Science

Volume 25 | Number 3 Article 2

7-7-2020

Temperature-Dependent Viscosity Effect on the Peristaltic Transport of (MHD) Blood Flow Ree-Eyring Fluid Through Porous Medium inAn Asymmetric Channel

Rasha Yousif Hassen
University of Technology, Department of Science, Mathematics and application of computer,
rashamath80@yahoo.com

Hayat Adil Ali
University of Technology, Department of Science, Mathematics and application of computer,
100048@uotechnology.edu.iq

Recommended Citation

Hassen, Rasha Yousif and Ali, Hayat Adil (2020) "Temperature-Dependent Viscosity Effect on the Peristaltic Transport of (MHD) Blood Flow Ree-Eyring Fluid Through Porous Medium inAn Asymmetric Channel," *Al-Qadisiyah Journal of Pure Science*: Vol. 25: No. 3, Article 2.
DOI: 10.29350/qjps.2012.17.3.1118
Available at: https://qjps.researchcommons.org/home/vol25/iss3/2

Al-Qadisiyah Journal of Pure Science
ISSN(Printed): 1997-2490 ISSN(Online): 2411-3514
DOI: /10.29350/jops.

Temperature-Dependent Viscosity Effect on the Peristaltic Transport of (MHD) Blood Flow Ree-Eyring Fluid Through Porous Medium in An Asymmetric Channel

Authors Names
a. Rasha Yousif Hassen
b. Hayat Adil Ali

Article History
Received on: 9/4/2020
Revised on: 1/5/2020
Acceptedon:13/5/2020

Keywords:
Temperature-dependent viscosity effect
Ree-Eyring fluid
Asymmetric channel

DOI:
https://doi.org/10.29350/
jops.2020.25. 3.1118

ABSTRACT

In this article, the peristaltic transport of blood flow Ree-Eyring electrically conducting fluid in a porous medium under the effect of magnetohydrodynamic and temperature dependent viscosity through an asymetric channel is examined. Governing flow problem are based on momentum and energy equations are mathematically modelled and investigated in a wave frame of reference moving with the velocity of the wave, by considering the assumption of long wavelength approximation compared to small Renold's number they simplified and reduced into couple partial differential equations. Exact solution for the temperature profile has been obtained whereas perturbation method employed to find the approximate solution for the stream function. The impact of important physical pertinent parameters on flow phenomena are discussed graphically. The graphs depict that the dimensionless viscosity parameter has a mixed effect on velocity profile moreover the two Ree-Eyring fluid parameters A and W has an opposite influence on the velocity profile.

MSC:

1. Introduction

During many years before, the study of peristaltic flows has been carried out much of importance in physiology and biomedical industry. The peristaltic transport can be defined as a fluid mechanism transport by way of area of sinusoidal waves. This type of such flows can be observed at most in a human body like (food swallowing process, the urine movement from kidney to the bladder and the blood flow through a small vessel in human circulator system), which gained a large attention because of its senior importance in physiological are mentioned in literatures [6,12,15].

a University of Technology, Department of Science, Mathematics and application of computer Email: rashamath80@yahoo.com
b University of Technology, Department of Science, Mathematics and application of computer Email: 100048@uotechnology.edu.iq

It's important to observe that the fluid concerned in the necessary applications is non-Newtonian and such materials flow are those whose viscosity depends onto the deformation rate like (blood, molasses, silicon oils, polymer solutions, printer ink, sand in water, soap solutions, biological fluids, personal care products, food products, building materials, etc.) see refs [2,8].

To the best of our knowledgment, Recently The magneto hydrodynamic (MHD) flow in peristaltic transport of fluid takes a major attention of several researchers, because of its helpful role in an industrial process such as (petroleum industries, designing of MHD power generators and helps to cure some of the diseases such as cancer by using the magnetic drug target). Moreover, it is widely used in blood filtration devices, it is useful to control blood flow, design blood pumps, heart lung machine, and many other processes, so in refs [4,5,7,9-14,16-18] have been investigated different effects on magneto hydrodynamic (MHD) peristaltic flow.

The viscosity in general is taken as constant; rarely, the viscosity considered as temperature dependent only in cases like higher temperature difference and viscous dissipation, see refs. [1,3]. in this work, we search in our work the influence of temperature-dependent viscosity on peristaltic transport of (MHD) blood Ree-Eyring fluid through a porous medium in an asymmetric channel. Also, we taken into consideration the long wave number and low Renolds number to simplify the problem. The perturbation method is used to find the last frame of the stream function. Finally, the results presented show the effects of various parameters on the velocity, temperature distribution, pressure gradient, pressure rise and stream function, all the results have been discussed graphically.

2. Mathematical Modeling

We introduced the peristaltic transport of incompressible Ree-Eyring fluid through an inclined asymmetric channel with a total width $(d_1 + d_2)$. The flow is characterized by the existence of (MHD) field. A Reynolds number is taken small and the induced magnetic wave number δ is neglected. The flow which is given by the peristaltic waves of length λ moving with a constant speed c along the channel walls.

Geometry of the walls surfaces are given by

$$Y_1 = H_1(\bar{X}, t) = d_1 + a_1 sin\left(\frac{2\pi(\bar{X}-ct)}{\lambda}\right) \quad \dots (1)$$

$$Y_2 = H_2(\bar{X}, t) = -d_2 - a_2 sin[\left(\frac{2\pi(\bar{X}-ct)}{\lambda}\right) + \emptyset] \quad \dots (2)$$

Where $Y_1 and\ Y_2$ are the right and the left side of the wall respectively, $d_1 and\ d_2$t are the non-uniform parameters, $a_1 and\ a_2$ are the wave amplitudes, t is the time and $(\bar{X}, \bar{Y})$ the rectangular coordinates in a fixed frame. $\emptyset$ is the phase difference and $\emptyset \in [0, \pi]$ such that when $\emptyset = 0$ corresponds to asymmetric channel with waves out of phase, and when $\emptyset = \pi$, the waves in phase. Further $a_1, a_2, d_1, d_2\ and\ \emptyset$ satisfy the important condition

$$a_1{}^2 + a_2{}^2 + 2a_1 a_2 d_1\, d_2 cos\emptyset \leq (d_1 + d_2)^2. \quad \dots (3)$$

The fluid satisfies Ree-Eyring model and its extra stress tensor is given as follows

$$\overline{S_{ij}} = \mu(T)\frac{\partial \bar{V}_i}{\partial \bar{X}_j} + \frac{1}{\beta}\sinh^{-1}\frac{\partial \bar{V}_i}{c_1 \partial \bar{X}_j} \qquad \dots (4)$$

where

$$\sinh^{-1}\frac{\partial \bar{V}_i}{c_1 \partial \bar{X}_j} \approx \frac{1}{c_1}\frac{\partial \bar{V}_i}{\partial \bar{X}_j} - \frac{1}{6{c_1}^3}\left(\frac{\partial \bar{V}_i}{\partial \bar{X}_j}\right)^3 \qquad \dots (5)$$

and

$$S_{ij} = \left(\mu(T) + \frac{1}{\beta c_1}\right)\frac{\partial \bar{V}_i}{\partial \bar{X}_j} - \frac{1}{6\beta {c_1}^3}\left(\frac{\partial \bar{V}_i}{\partial \bar{X}_j}\right)^3 \qquad \dots (6)$$

$\mu(T)$ Is the dynamic variable viscosity.

The fundamental equations of the flow can be written as below:

$$\frac{\partial \mathrm{u}}{\partial \mathrm{x}} + \frac{\partial v}{\partial y} = 0 \qquad \dots (7)$$

X-component of momentum equation

$$\rho\left(\frac{d\bar{U}}{dt} + \bar{U}\frac{\partial \bar{U}}{\partial \bar{X}} + \bar{V}\frac{\partial \bar{U}}{\partial \bar{Y}}\right) = -\frac{\partial \bar{P}}{\partial \bar{X}} + \frac{\partial \bar{S}_{\bar{X}\bar{X}}}{\partial \bar{X}} + \frac{\partial \bar{S}_{\bar{X}\bar{Y}}}{\partial \bar{Y}} - \sigma {\beta_0}^2(\bar{U}) - \frac{\mu(T)}{\kappa}\bar{U} \qquad \dots (8)$$

Y-component of momentum equation

$$\rho\left(\frac{d\bar{V}}{dt} + \bar{U}\frac{\partial \bar{V}}{\partial \bar{X}} + \bar{V}\frac{\partial \bar{V}}{\partial \bar{Y}}\right) = -\frac{\partial \bar{P}}{\partial \bar{Y}} + \frac{\partial \bar{S}_{\bar{X}\bar{Y}}}{\partial \bar{X}} + \frac{\partial \bar{S}_{\bar{Y}\bar{Y}}}{\partial \bar{Y}} - \sigma {\beta_0}^2(\bar{V}) - \frac{\mu(T)}{\kappa}\bar{V} \qquad \dots (9)$$

and energy equation with heating effect is

$$\rho c_P\left(\frac{\partial T}{\partial \bar{t}} + \bar{U}\frac{\partial T}{\partial \bar{X}} + \bar{V}\frac{\partial T}{\partial \bar{Y}}\right) = K\left(\frac{\partial^2 T}{\partial \bar{X}^2} + \frac{\partial^2 T}{\partial \bar{Y}^2}\right) - \frac{\partial}{\partial \bar{Y}}q_r + \varphi \qquad \dots (10)$$

Where

$$q_r = \frac{16\,\sigma^* {T_0}^3}{3K^*}\frac{\partial T}{\partial \bar{Y}} \qquad \dots (11)$$

In which σ is the electrical conductivity, K is the thermal conductivity, $\sigma^*$and K^* are the Stefan Boltzman constant and the mean absorption coefficient respectively, κ porosity parameter, ρ density and c_P specific heat.

The corresponding boundary conditions are

$$\left.\begin{aligned} T = T_0\,, u = 0\,, \psi = \frac{F}{2} \quad & at \quad \bar{Y} = H_1 \\ T = T_1\,, u = 0\,, \psi = -\frac{F}{2} \quad & at \quad \bar{Y} = H_2 \end{aligned}\right\}. \qquad \dots (12)$$

In which $T_0 and\, T_1$ are the temperature at the right and left walls coefficient respectively.

Normalizing flow equations (7) - (12) from laboratory to the steady frame using the quantities:

$$\bar{X} = \bar{x} - ct, \bar{U} = \bar{u} - c, \bar{V} = \bar{v}, T = T, \bar{P} = \bar{p}, \bar{Y} = \bar{y} \qquad \dots (13)$$

Fluid fundamental equations will be such as below

$$\frac{\partial \mathrm{u}}{\partial \mathrm{x}} + \frac{\partial v}{\partial y} = 0 \qquad \ldots (14)$$

X-component of momentum equation:

$$\rho\left((\bar{U}+c)\frac{\partial \bar{U}}{\partial \bar{X}} + \bar{v}\frac{\partial \bar{U}}{\partial \bar{Y}}\right) = -\frac{\partial \bar{P}}{\partial \bar{X}} + \frac{\partial \bar{S}_{\bar{X}\bar{X}}}{\partial \bar{X}} + \frac{\partial \bar{S}_{\bar{X}\bar{Y}}}{\partial \bar{Y}} - \sigma {\beta_0}^2(\bar{u}+c) - \frac{\mu(T)}{\kappa}(\bar{u}+c) \qquad \ldots (15)$$

Y-component of momentum equation:

$$\rho\left((\bar{U}+c)\frac{\partial \bar{V}}{\partial \bar{X}} + \bar{v}\frac{\partial \bar{V}}{\partial \bar{Y}}\right) = -\frac{\partial \bar{P}}{\partial \bar{Y}} + \frac{\partial \bar{S}_{\bar{X}\bar{Y}}}{\partial \bar{X}} + \frac{\partial \bar{S}_{\bar{Y}\bar{Y}}}{\partial \bar{Y}} - \sigma {\beta_0}^2 \bar{v} - \frac{\mu(T)}{\kappa}\bar{V} \qquad \ldots (16)$$

$$\rho c_P\left((\bar{U}+c)\frac{\partial T}{\partial \bar{X}} + \bar{V}\frac{\partial T}{\partial \bar{Y}}\right) = K\left(\frac{\partial^2 T}{\partial \bar{X}^2} + \frac{\partial^2 T}{\partial \bar{Y}^2}\right) - \frac{\partial}{\partial \bar{Y}} q_r + \varphi \qquad \ldots (17)$$

Now by using the following dimensionless quantities

$$x = \frac{\bar{X}}{\lambda}, y = \frac{\bar{y}}{d_1}, u = \frac{\bar{u}}{c}, v = \frac{\lambda \bar{v}}{d_1 c}, h_1 = \frac{H_1}{d_1}, h_2 = \frac{H_2}{d_1}, p = \frac{{d_1}^2 \bar{p}}{\lambda \mu c}, \delta = \frac{d_1}{\lambda}, \beta_1^* = \frac{\beta_1}{d_1}, S = \frac{d_1 \bar{S}(\bar{X})}{\mu c}, Re = \frac{\rho c d_1}{\mu}, \theta = \frac{T - T_0}{T1 - T_0}, Pr = \frac{\mu c_P}{k}, H = \beta_0 d_1 \sqrt{\frac{\sigma}{\mu}}, \mathrm{B} = \frac{\varphi\, {d_1}^2}{k(\Delta T)}, a = \frac{a_1}{d_1}, b = \frac{a_2}{d_1}, Rn = \frac{16\, \sigma^* {T_0}^3}{3\, k^* \kappa}, \mu(\theta) = \frac{\mu(T)}{\mu}, d = \frac{d_2}{d_1}, W = \frac{1}{\mu \beta c_1}, A = \frac{W}{6 \beta c_1} \qquad \ldots (18)$$

Where $h_1 and\, h_2$ are the dimensionless right and left walls surface, x, y, u, v components of the dimensionless coordinates, axial velocity, transverse component of velocity, δ is the wave number, Re is the Reynolds number, θ is the temperature distribution vector, Pr Prandtl number, H is the Hartman number, B is the heat generation parameter, Rn is thermal radiation parameter, note that we omitted asterisks for simplicity.

Defining the stream function $\psi(x, y, t)$ by $u = \psi_y,\ v = -\delta \psi_x$

Applying Eqs. (18) Into Eqs. (12) – (17) and making use of stream function. Flow equations have the following form

$$\delta Re\left(-(\psi_y + 1)\psi_{xy} - \delta \psi_x \psi_{xy}\right) = -P_x + \delta \frac{\partial S_{xx}}{\partial x} + \frac{\partial S_{xy}}{\partial y} - H^2(\psi_y + 1) - \frac{\mu(\theta)}{\kappa}(\psi_y + 1)$$
$$\ldots (19)$$

$$\delta^3 Re\left(-(\psi_y + 1)\psi_x - \psi_x \psi_{xy}\right) = -P_y + \delta \frac{\partial S_{yy}}{\partial y} + \delta^2 \frac{\partial S_{yx}}{\partial x} + \delta^2 \frac{\mu(\theta)}{\kappa}\psi_x + \delta^2 H^2 \psi_x$$
$$\ldots (20)$$

$$\delta Re Pr\left((\psi_y + 1)\frac{\partial \theta}{\partial x} - \psi_x \frac{\partial \theta}{\partial y}\right) = \delta^2 \frac{\partial^2 \theta}{\partial x^2} + \frac{\partial^2 \theta}{\partial y^2} - Rn \frac{\partial^2 \theta}{\partial y^2} + \mathrm{B} \qquad \ldots (21)$$

Espousing the supposition of peristaltic long wavelength and low Reynolds number, Eqs. (19)- (21) will be reduced to the following form

$$P_x = \frac{\partial S_{xy}}{\partial y} - H^2(\psi_y + 1) - \frac{\mu(\theta)}{\kappa}(\psi_y + 1), \qquad \ldots (22)$$

$$P_y = 0, \qquad \ldots (23)$$

$$\frac{\partial^2\theta}{\partial y^2} - Rn\frac{\partial^2\theta}{\partial y^2} + \mathrm{B} = 0, \qquad \ldots (24)$$

From Eq. (6), we obtain

$$\left.\begin{aligned} S_{xy} &= \left(\mu(\Theta) + \frac{1}{\mu\beta c}\right)\psi_{yy} - \frac{1}{6\beta\mu c{d_1}^2}\left(\psi_{yy}\right)^3 \\ S_{yx} &= \left(\mu(\Theta) + \frac{1}{\mu\beta c}\right)\psi_{yy} - \frac{1}{6\beta\mu c{d_1}^2}\left(\psi_{yy}\right)^3 \end{aligned}\right] \quad \ldots (25)$$

$$S_{xx} = \delta\left(\mu(\Theta)\psi_{xy} + \frac{1}{\beta c}\psi_{xy} - \frac{1}{6\beta\mu c\lambda^2}\left(\psi_{xy}\right)^3\right)$$

$$S_{yy} = \delta\left(-\mu(\Theta)c\delta\psi_{xy} - \delta\frac{1}{\mu\beta}\psi_{xy} + \frac{1}{6\beta\mu\lambda^2}\left(\delta\psi_{xy}\right)^3\right)$$

$$S_{xx} = 0, S_{yy} = 0 \qquad \ldots (26)$$

Connected with the following dimensionless temperature and velocity conditions

$$\left.\begin{aligned} \theta = 0\ , \psi = \frac{F}{2} \qquad & at\ y = h_1 \\ \theta = 1\ , \psi = \frac{-F}{2} \qquad & at\ y = \ h_2 \\ u = -1\ \ & at\ \ y = h_1, h_2 \end{aligned}\right]. \qquad \ldots (27)$$

Where

$$h_1 = 1 + a\,(sin(2\pi x))\,,\ h_2 = -d - b(sin(2\pi x + \emptyset))$$

Furthermore, through Eqs. (22) And (23), we obtain

$$\frac{\partial^2 S_{xy}}{\partial y^2} - H^2\left(\psi_{yy}\right) - \frac{\partial}{\partial y}\left(\frac{\mu(\theta)}{\kappa}\left(\psi_y + 1\right)\right) = 0 \qquad \ldots (28)$$

Put a dimensionless approximate expression for $\mu(\theta)$ such [8]

$\mu(\theta) = e^{-\epsilon\theta} = 1 - \epsilon\theta$, where $\epsilon < 1$,

ϵ Is a non- dimensional viscosity parameter.

The instantaneous volume flow rate in the laboratory frame is given as

$$Q = \int_{H_1}^{H_2} \overline{U}(\bar{X}, \bar{Y}, t)d\bar{Y} \qquad \ldots (29)$$

Eq. (29) rewritten in wave frame as

$$q = \int_{h_1}^{h_2} \bar{u}(\bar{x}, \bar{y})d\bar{y} \qquad \ldots (30)$$

Using Eq. (13), the relationship between the two expressions is

$$Q = q + c(h_1(\bar{x}) - h_2(\bar{x})) \quad \ldots (31)$$

The time mean flow over a period $T_1 = (\lambda/c)$ at fixed frame is derived as

$$\breve{Q} = \frac{1}{T_1}\int_0^{T_1} Q dt \qquad \ldots (32)$$

Integrating the above equation and using Eq. (30), yields

$$\Phi = q + c(d_1 + d_2) \qquad \ldots (33)$$

Introducing the dimensionless time mean flows, Φ and F, in fixed and wave frame, respectively as

$$\Phi = \frac{\breve{\mathrm{Q}}}{\mathrm{cd}_1}, \text{and } F = \frac{q}{cd_1} \quad \ldots (34)$$

In the fixed and moving frames, we can write Eq. (33) as

$$\Phi = \mathrm{F} + d + 1 \qquad \ldots (35)$$

Where

$$F = \int_{h_1(x)}^{h_2(x)} u(x,y)dy$$

The non- dimensional pressure rise Δp is obtained by the following expression

$$\Delta p = \int_0^1 \frac{dp}{dx} dx \qquad \ldots (36)$$

3. Solution Technique

We have two different ways to solve our equations are mentioned below:

3.1 Exact Solution

The temperature equation is solved exactly by integrating Eq. (24) twice with respect to y as below

$$\theta = -\frac{y^2\mathrm{B}}{2} + r_1 + y\mathrm{r}_2.$$

Where

$$\mathrm{r}_1 = -\frac{2\mathrm{h}_2 + {\mathrm{h}_1}^2\mathrm{h}_2\mathrm{B} - \mathrm{h}_1{\mathrm{h}_2}^2\mathrm{B}}{2(\mathrm{h}_1 - \mathrm{h}_2)},$$

$$r_2 = -\frac{2 + {\mathrm{h}_1}^2\mathrm{B} - {\mathrm{h}_2}^2\mathrm{B}}{2(-\mathrm{h}_1 + \mathrm{h}_2)},$$

3.2 Perturbation Method

We used the perturbation method for small non- dimensional viscosity parameter ϵ and expanding the flow quantities in a power series of ϵ in the form

$$\psi = \psi_0 + \epsilon\,\psi_1 \qquad \ldots (37)$$

Substituting Eq. (37) in Eqs. (28) and (27), then comparing the coefficients of same power of ϵ up to the first order we obtain the following two systems

3.2.1 Zeroth order system

The general form of zeroth- order system is: -

$$(1+W)\,\psi_{0yyyy} - A\frac{\partial^2}{\partial y^2}\left(\psi_{0yy}\right)^3 - \left(H^2+\frac{1}{\kappa}\right)\psi_{0yy} = 0 \qquad \dots (38)$$

Now, we use the perturbation to ψ_0 again for small Ree-Eyring fluid parameter A as :

$$\psi_0 = \psi_{00} + A\psi_{01} + \cdots \qquad \dots (39)$$

Substituting Eq. (39) in Eq. (38) gives:

3.2.1.1 Zeroth order A^0

$$(1+W)\,\psi_{00yyyy} - \left(H^2+\frac{1}{\kappa}\right)\psi_{00yy} = 0 \qquad \dots (40)$$

3.2.1.2 First order A^1

$$(1+W)\,\psi_{01yyyy} - \frac{\partial^2}{\partial y^2}\left(\left(\psi_{00yy}\right)^3\right) - \left(H^2+\frac{1}{\kappa}\right)\psi_{01yy} = 0 \qquad \dots (41)$$

3.2.2 First order system ϵ^1

The general form of the first order system is

$$(1+W)\,\psi_{1yyyy} - \theta\,\psi_{0yyyy} - 2\frac{\partial\theta}{\partial y}\,\psi_{0yyy} - \frac{\partial^2\theta}{\partial y^2}\,\psi_{0yy} - A\frac{\partial^2}{\partial y^2}\left(\left(\psi_{0yy}\right)^2\left(\psi_{1yy}\right)\right) - \left(H^2+\frac{1}{\kappa}\right)\psi_{1yy} + \frac{1}{\kappa}\frac{\partial\theta}{\partial y}\left(\psi_{0y}+1\right) + \frac{\theta}{\kappa}\,\psi_{0yy} = 0 \quad \dots (42)$$

By using the perturbation to A again as follows

$$\psi_1 = \psi_{10} + A\psi_{11} \qquad \dots (43)$$

Substituting Eq. (43) in Eq. (42) gives:

3.2.2.1 Zeroth order for ϵ^1, A^0

$$(1+W)\,\psi_{10yyyy} - \theta\,\psi_{00yyyy} - \left(H^2+\frac{1}{\kappa}\right)\psi_{10yy} + \frac{\theta}{\kappa}\,\psi_{00yy} + \frac{1}{\kappa}\frac{\partial\theta}{\partial y}\left(\psi_{00y}+1\right) - \theta\,\psi_{00yyyy} - 2\frac{\partial\theta}{\partial y}\,\psi_{00yyy} - \frac{\partial^2\theta}{\partial y^2}\,\psi_{00yy} = 0 \qquad \dots (44)$$

3.2.2.2 First order for A^1

$$(1+W)\,\psi_{11yyyy} - \theta\,\psi_{01yyyy} - \frac{\partial^2}{\partial y^2}\left(\left(\psi_{00yy}\right)^2\left(\psi_{10yy}\right)\right) - \left(H^2+\frac{1}{\kappa}\right)\psi_{11yy} + \frac{\theta}{\kappa}\,\psi_{01yy} + \frac{1}{\kappa}\frac{\partial\theta}{\partial y}\left(\psi_{01y}+1\right) - 2\frac{\partial\theta}{\partial y}\,\psi_{01yyy} - \frac{\partial^2\theta}{\partial y^2}\,\psi_{01yy} = 0 \qquad \dots (45)$$

Solving the both of systems using Mathematica program we get the closed form for ψ

$$\psi = \psi_{00} + A\psi_{01} + \epsilon(\psi_{10} + A\psi_{11})\,.$$

Where

$$\psi_{00} = \frac{e^{-\xi y}(e^{2\xi y}c_1 + c_2)}{v^2} + c_3 + yc_4,$$

$$\psi_{10} = c_{11} + yc_{12} + K_1(-e^{2\xi y}B_1(A_2+A_3) + A_4)\,,$$

$$\psi_{11} = K_2(D_1 + D_2 + D_3 + D_4 + D_5 + D_6 + D_7 + D_8 + D_9 + D_{10} + D_{11} + D_{12} + D_{13} + D_{14}) + c_{15} + yc_{16}.$$

In which

$$A_1 = \frac{(18e^{4\xi y}(-5+2\xi y)c_1^2c_2+18e^{2\xi y}(5+2\xi y)c_1c_2^2-c_2^3))}{24\xi^3(1+W)}$$

$$L_1 = \frac{(e^{-3\xi y}(24e^{2\xi y}\xi(e^{2\xi y}c_5+c_6)+e^{6\xi y}c_1^3)}{24\xi^3(1+W)}$$

$$K_1 = \frac{1}{48\xi^6\kappa}e^{-\xi y},$$

$$A_2 = \left(-e^{2\xi y}\left(45-42vy+3\xi^2(6y^2-\kappa)-6\xi^4y^2\kappa+4\xi^5y^3\kappa+\xi^3(-4y^3+6y\kappa)\right)c_1\right),$$

$$A_3 = \left(-45-42\xi y+6\xi^4y^2\kappa+4\xi^5y^3\kappa+3\xi^2(-6y^2+\kappa)+\xi(-4y^3+6y\kappa)\right)c_2 - 8e^{\xi y}\xi^4y^3c_4),$$

$$A_4 = 6\xi\left(e^{2\xi y}c_1\left(2\xi(-5+2\xi y)(-1+\xi^2\kappa)r_1+\left(-7+6\xi y-2\xi^3y\kappa+2\xi^4y^2\kappa-\xi^2(2y^2+3\kappa)\right)r_2\right)+c_2\left(-2\xi(5+2\xi y)(-1+\xi^2\kappa)r_1+\left(7+6\xi y-2\xi^3y\kappa-2\xi^4y^2\kappa+\xi^2(2y^2+3\kappa)\right)r_2\right)+4\xi^3\left(2\kappa\left(e^{2\xi y}c_9+c_{10}\right)\right)+e^{\xi y}y^2c_4r_2\right),$$

$$\xi = \sqrt{\left(H^2+\frac{1}{\kappa}\right)},\ B_1 = \frac{1}{(1+Rn)}$$

$$K_2 = \frac{1}{27648\xi^7\kappa}e^{-3\xi y},$$

$$D_1 = -B_1(e^{6\xi y}\left(-115+3\xi(-171+52y)-9\xi^2(-36y+8y^2-63\kappa)+648\xi^5y^2\kappa+\right.$$
$$\left.,288\xi^6y^3\kappa+27(8y^2+7\kappa-36y\kappa)-36\xi^4y(8y^2+21\kappa-18y\kappa)\right){c_1}^3$$

$$D_2 = 288e^{2\xi y}\left(621+3\xi(7+198y)+18\xi^2(y+15y^2-\kappa)+\xi^7y^4\kappa-\xi^6y^3(16+9y)\kappa+\xi^4y(4y^2+9y^3-12\kappa-36y\kappa)+\xi^3(9y^2+72y^3+6\kappa-36y\kappa)-\right.$$
$$\left.,\xi^5y^2(y^2+21\kappa+24y\kappa)\right){c_1}{c_2}^2$$

$$D_3 = \left(115+3\xi(-171+52y)+9\xi^2(-36y+8y^2-63\kappa)+648\,\xi^5y^2\kappa-\right.$$
$$\left.,288\xi^6y^3\kappa+27\xi^3(8y^2+7\kappa-36y\kappa)+36\xi^4y(8y^2+21\kappa-18y\kappa)\right){c_2}^3$$

$$,D_4 = 3072e^{\xi y}\xi^2(4+3\xi y){c_2}^2c_4$$

$$D_5 = 96e^{4\xi y}{c_1}^2\left(-621+3\xi(7+198y)-18\xi^2(y+15y^2-\kappa)+\xi^6y^3(16+9y)\kappa+\xi^3(9y^2+72y^3+6\kappa-36y\kappa)-\xi^5y^2(y^2+21\kappa+24y\kappa)+\xi^4y(-4y^2-9y^3+12\kappa+\right.$$
$$\left.,36y\kappa)\right)c_2+32e^{\xi y}\xi^2(-4+3\xi y)c_4)$$

$$D_6 = 576e^{2\xi y}\xi\left(e^{2\xi y}\left(45-42\xi y+3\xi^2(6y^2-\kappa)-6\xi^4y^2\kappa+4\xi^5y^3\kappa+\xi^3(-4y^3+\right.\right.$$
$$\left.\left.6y\kappa)\right)c_5+\left(45+42\xi y+3\xi^2(6y^2-\kappa)-6\xi^4y^2\kappa-4\xi^5y^3\kappa+\xi^3(4y^3-6y\kappa)\right)c_6+\right.$$
$$\left.,8e^{\xi y}\xi^4y^3c_8)\right)$$

$$D_7 = 12(e^{6\xi y}\xi{c_1}^3\left(12\xi\left(-1+15\xi-15\xi^3\kappa+12\xi^4y\kappa+\xi^2(-12y+9\kappa)\right)r_1+\right.$$
$$\left.\left(13-3\xi(-9+4y)+9\xi^2(4y-9\kappa)+108y\kappa\xi^4+72\xi^5y^2\kappa-9\xi^3(8y^2+23\kappa-\right.\right.$$
$$\left.\left.,12y\kappa)\right)r_2\right)$$

$$D_8 = \xi{c_2}^3\left(-12\xi\left(-1-15\xi+15\xi^3\kappa+12\xi^4y\kappa+\xi^2(-12y+9\kappa)\right)r_1+\left(13+\right.\right.$$
$$\left.\left.,3\xi(-9+4y)+9\xi^2(4y-9\kappa)+108\xi^4y\kappa-72\xi^5y^2\kappa+9\xi^3(8y^2+23\kappa-12y\kappa)\right)r_2\right)$$

$$,D_9 = -96{c_2}^2\left(6e^{2\xi y}\xi^5(5+2\xi y)\kappa c_9 - 3\xi^5\kappa c_{10} - 2e^{\xi y}c_4 r_2\right)$$

$$D_{10} = 24e^{4\xi y}c_1^2\big(12e^{2\xi y}\xi^5\kappa c_9 + 24\xi^5(-5+2\xi y)\kappa c_{10} - 396\xi^2 c_2 r_1 - 72\xi^3 c_2 r_1 + 216\xi^3 y c_2 r_1 + 48\xi^4 y c_2 r_1 - 36\xi^4 y^2 c_2 r_1 - 12\xi^5 y^2 c_2 r_1 + 36\xi^4\kappa c_2 r_1 + 72\xi^5\kappa c_2 r_1 - 72\xi^5 y\kappa c_2 r_1 - 48\xi^6 y\kappa c_2 r_1 + 36\xi^6 y^2\kappa c_2 r_1 + 12\xi^7 y^2\kappa c_2 r_1 + 459\xi c_2 r_2 + 15\xi^2 c_2 r_2 - 414\xi^2 y c_2 r_2 + 18\xi^3 y c_2 r_2 + 162\xi^3 y^2 c_2 r_2 - 12\xi^4 y^2 c_2 r_2 - 24\xi^4 y^3 c_2 r_2 - 4\xi^5 y^3 c_2 r_2 + 9\xi^3\kappa c_2 r_2 - 39\xi^4\kappa c_2 r_2 + 54\xi^4 y\kappa c_2 r_2 - 66\xi^5 y\kappa c_2 r_2 - 54\xi^5 y^2\kappa c_2 r_2 + 48\xi^6 y^2\kappa c_2 r_2 + ,24\xi^6 y^3\kappa c_2 r_2 + 4\xi^7 y^3\kappa c_2 r_2 + 8e^{\xi y}c_4 r_2\big)$$

$$D_{11} = 24e^{2\xi y}\xi c_1 c_2(48e^{2\xi y}\xi^4(-5+2\xi y)\kappa c_9 - 48\xi^4(5+2\xi y)\kappa c_{10} + c_2(12\xi(33 + 6\xi(-1+3y) + \xi^2(-4y+3y^2-3\kappa) + \xi^4(4-3y)y\kappa + \xi^5 y^2\kappa - \xi^3(y^2 - 6\kappa + ,6y\kappa))r_1$$

$$D_{12} = (459 + 3\xi(-5+138y) + 4\xi^6 y^3\kappa - 24\xi^5 y^2(2+y)\kappa + 9\xi^2(2y+18y^2+\kappa) + ,3\xi^3(4y^2+8y^3+13\kappa-18y\kappa) - 2\xi^4 y(2y^2+33\kappa+27y\kappa))r_2))$$

$$D_{13} = 288e^{2\xi y}\xi^2(e^{2\xi y}c_5(2\xi(-5+2\xi y)(-1+\xi^2\kappa)r_1 + (-7+6\xi y - 2\xi^3 y\kappa + ,2\xi^4 y^2\kappa - \xi^2(2y^2+3\kappa))r_2)$$

$$D_{14} = c_6(-2\xi(5+2\xi y)(-1+\xi^2\kappa)r_1 + (7+6\xi y - 2\xi^3 y\kappa - 2\xi^4 y^2\kappa + \xi^2(2y^2 + . 3\kappa))r_2) + 4\xi^3(2\kappa(e^{2\xi y}c_{13} + c_{14}) + e^{\xi y}y^2 c_8 r_2)))$$

And

$c_1, c_2, c_3, c_4, c_5, c_6, c_7, c_8, c_9, c_{10}, c_{11}, c_{12}, c_{13}, c_{14}, c_{15}, c_{16}$ can be found By applying the boundary conditions using simple calculations.

4. Result and Discussions

In this section, we displayed graphically the effect of different physical parameters on velocity profile, temperature distribution, pressure rise, pressure gradient. In addition, the stream function that corresponds to a specific situation for Ree-Eyring. The solutions of the temperature distributions have been found analytically, while for finding the velocity, temperature distribution, stream function, pressure gradient and pressure rise we employed a method of perturbation by using the software MATHEMATICA.

4.1. Velocity distribution

This part shows the behavior of velocity distribution with the following parameters $(H, A, \kappa, W, B, \epsilon)$ and for fixed values of $(a = 0.01, b = 0.1, \mathrm{d}_2 = 0.3, \mathrm{Rn} = 0.3, \phi = \frac{\mathrm{Pi}}{6}, x = 0.1, \Phi = 0.1)$ are investigated graphically. The graphs depict that the velocity profile is a concave downward also we noticed that the magnitude of velocity reach a fixed value in the central part of the channel, figure 1(a) is plotted to describe the action of Hartman number H on velocity distribution it shows that the velocity axial is a decreasing behavior toward the walls while a certain magnitude is seen in the range$(-0.2 \le x \le 1.1)$. Similar observation is seen for different values of the Ree-Eyring parameter A see figure 1(b) While it turns out from figure 2(a), 2(b) and figure 3(a) that the impact of permeability parameter κ, the Ree-Eyring parameter W and B are same i.e. they have an increment action on $u(y)$ near the right and left walls.

Whereas figure 3(b) reveals that $u(y)$ increases near the left wall for ascending magnitude of ϵ non- dimensional viscosity parameter while it decreases near the right wall and its value keeps fixed in the central part.

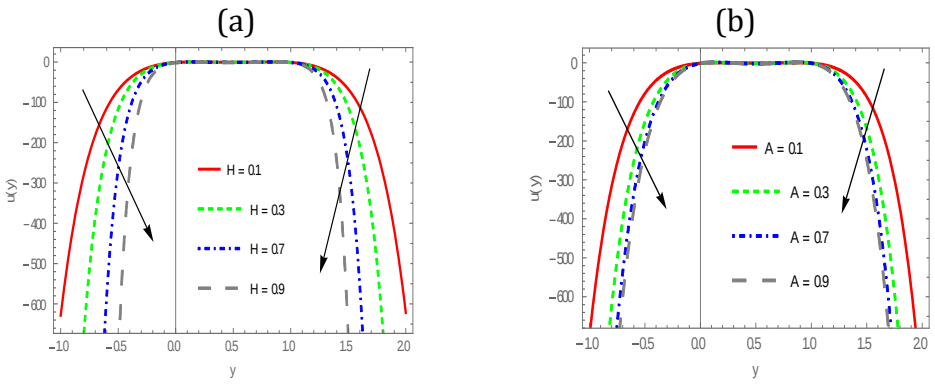

Figure 1: Velocity distribution is for different values of (a) Hartman number H (b) Ree-Eyring parameter A and when $\{a = 0.01, b = 0.1, \mathrm{d}_2 = 0.3, \mathrm{Rn} = 0.3, \phi = \frac{\mathrm{Pi}}{6}, x = 0.1, \Phi = 0.1\}$

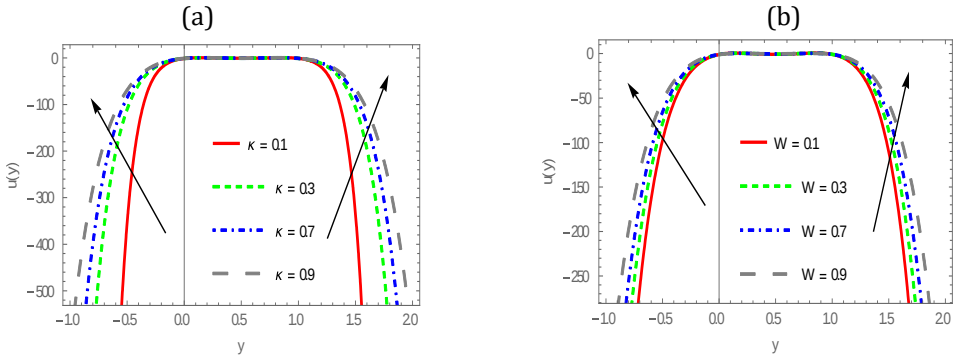

Figure 2: Velocity distribution is for different values of (a) permeability parameter κ (b) Ree-Eyring parameter W and when $\{a = 0.01, b = 0.1, \mathrm{d}_2 = 0.3, \mathrm{Rn} = 0.3, \phi = \frac{\mathrm{Pi}}{6}, x = 0.1, \Phi = 0.1\}$

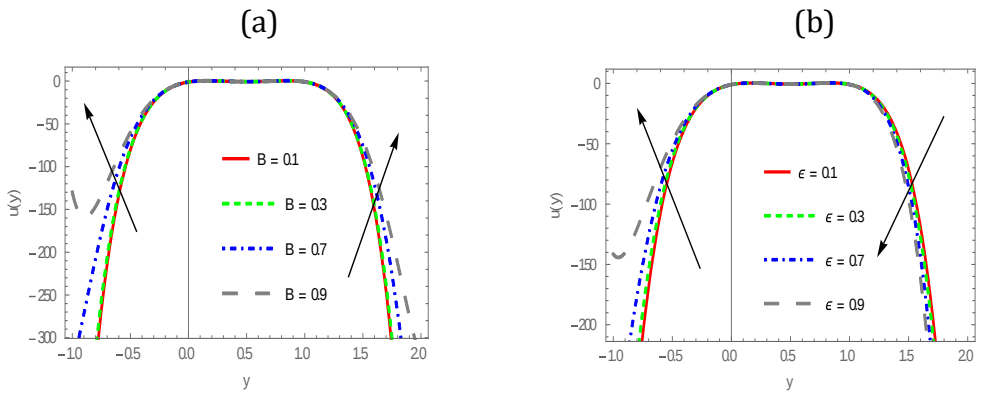

Figure 3: Velocity distribution is for different values of non-dimensional (a) heat source parameter B (b) viscosity parameter ϵ and when $\{a = 0.01, b = 0.1, \mathrm{d}_2 = 0.3, \mathrm{Rn} = 0.3, \phi = \frac{\mathrm{Pi}}{6}, x = 0.1, \Phi = 0.1\}$

4 .2 Pumping characteristics

In this part of work, the response in pressure gradient dp/dx and the pressure rise per wavelength Δp to various emerging parameters involving in our problem is present. Figures 4(a)-5(b) illustrate the variation in dp/dx against axial coordinate. Figures 4(a)-5(b), demonstrate two different observations for Ree-Eyring fluid parameter and Hartman number $W and\ H$, phase difference parameter $\emptyset$ and porous permeability κ variation respectively, we visualized from figures of dp/dx that the pressure gradient curve behaviors is an oscillatory in nature. Moreover some points of reflections on the dp/dx curves which opposite the state from increase to decrease and vice versa are depicted. We noticed that the enhancement of W and H values required modification in pressure gradient dp/dx in the central part of the channel to pass the same amount of fluid flux pass it more than near the right and left walls which means the flow can be easily passedwithout imposing much dp/dx in those regions, whereas opposite situations induced for ascending values of A and κ parameters.

The evolution of pressure rise per wavelength Δp_λ versus alteration in flow rate Φ is recorded in figures 6(a)-7(b) for fixed parameters $\left(a = 0.01, b = 0.1, \mathrm{d}_2 = 0.03, \mathrm{Rn} = 0.3, B = 0.4, \phi = \frac{\mathrm{Pi}}{3}, y = 0.1, d = 0.1, A = 0.4\right)$ and variation magnitude of(H, κ, ϵ, A). A linear relationship between Δp_λ and Φ is proven from these figures. Figure 6(a) exhibits elevation in pumping rate$(\Delta p_\lambda > 0, \Phi > 0)$, and retrograde pumping region $(\Delta p_\lambda > 0, \Phi < 0)$ however, a depressing in co-pumping region $(\Delta p_\lambda < 0, \Phi > 0)$ with enhancement of Hartman number$H$. While the rise in permeability parameter κ tends to damp pumping rate$(\Delta p_\lambda > 0)$, and retrograde pumping region $(\Phi < 0)$ whereas this behavior is reversed in co-pumping region see figure 6(b). Higher values of dimensionless viscosity parameter ϵ is a decreasing function on both regions pumping region and retrograde pumping but it is found an increment in the co-pumping region via Figure. 7(a). It is noted from figure 7(b) that an increase in Ree-Eyring fluid parameter W modified the retrograde pumping region $(\Delta p_\lambda > 0, \Phi < 0)$ and diminished co-pumping region$(\Delta p_\lambda < 0, \Phi > 0)$.

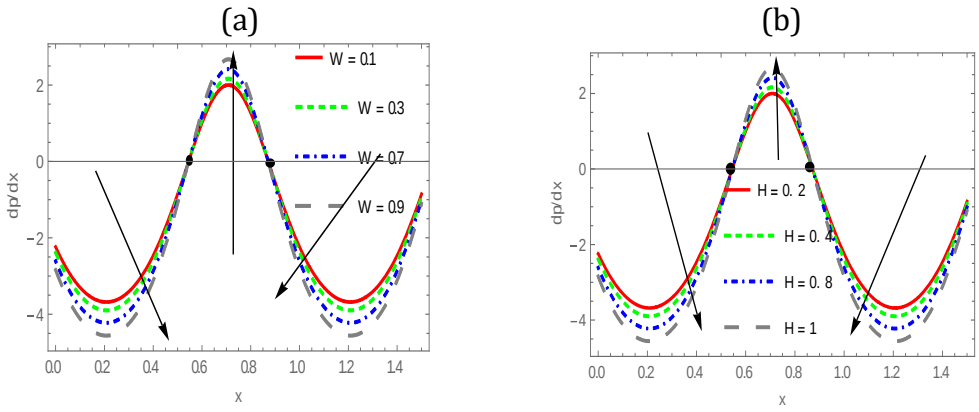

Figure 4: Pressure gradient versus axial distance x is for different values of (a) Ree-Eyring fluid parameter W (b) Hartman number H and when $\{a = 0.01, b = 0.1, \mathrm{d}_2 = 0.03, \mathrm{Rn} = 0.3, B = 0.4, \phi = \frac{\mathrm{Pi}}{3}, y = 0.1, d = 0.1, A = 0.4\}$

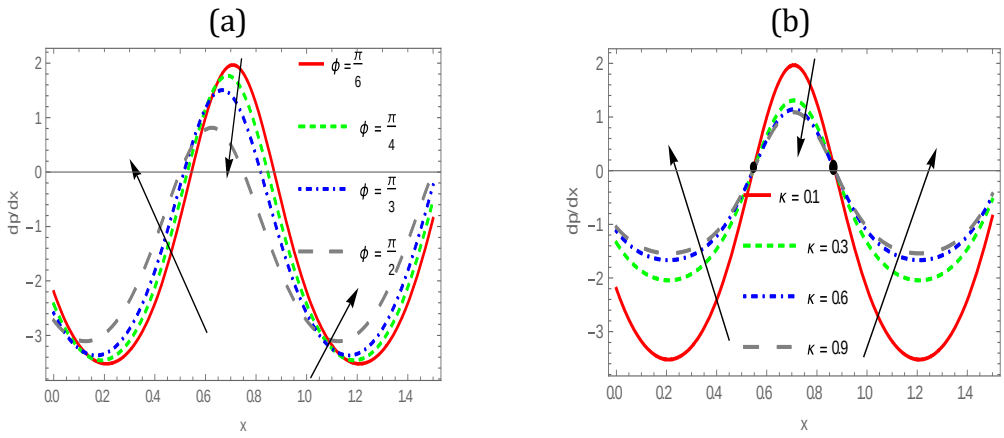

Figure 5: Pressure gradient versus axial distance x is for different values of (a) phase difference parameter ϕ (b) porosity parameter κ and when $\{a = 0.01, b = 0.1, \mathrm{d}_2 = 0.03, \mathrm{Rn} = 0.3, B = 0.4, \phi = \frac{\mathrm{Pi}}{3}, y = 0.1, d = 0.1, A = 0.4\}$

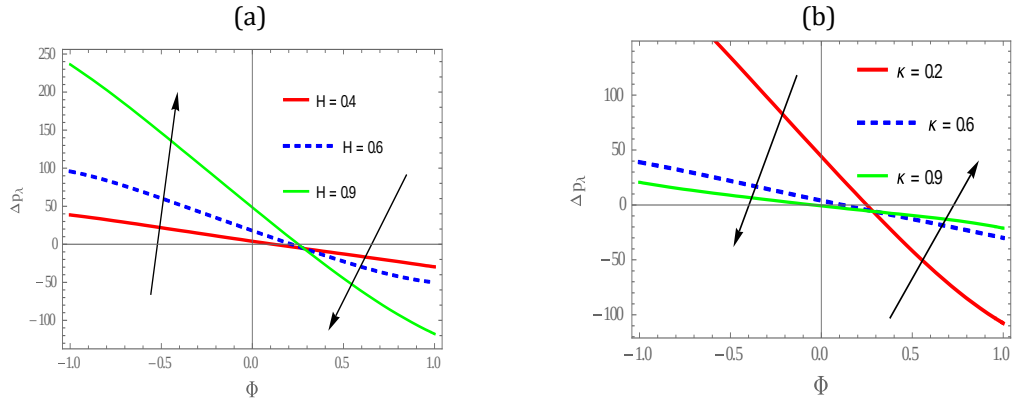

Figure 6: Pressure rise against flow rate Φ is for different values of (a) Hartman number H (b) porosity parameterκ and when $\{a = 0.01, b = 0.1, \mathrm{d}_2 = 0.03, \mathrm{Rn} = 0.3, B = 0.4, \phi = \frac{\mathrm{Pi}}{3}, y = 0.1, d = 0.1, A = 0.4\}$

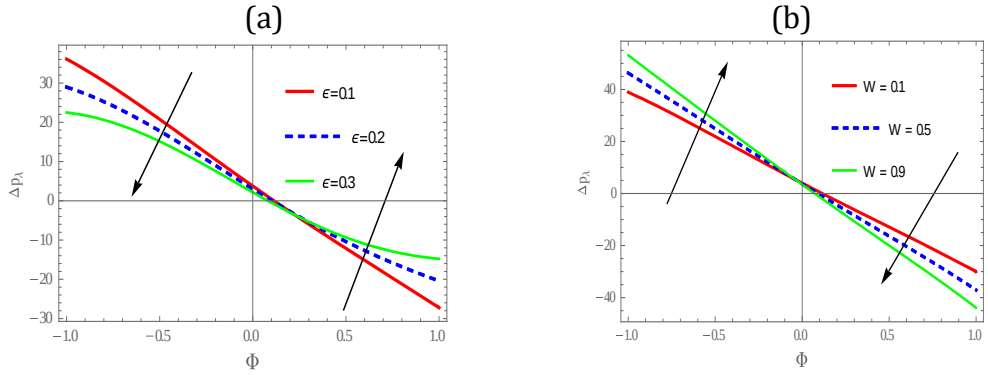

Figure 7: pressure rise is for different values of (a) dimensionless viscosity parameter ϵ (b) Ree-Eyring fluid parameter W and when $\{a = 0.01, b = 0.1, \mathrm{d}_2 = 0.03, \mathrm{Rn} = 0.3, B = 0.4, \phi = \frac{\mathrm{Pi}}{3}, y = 0.1, d = 0.1, A = 0.4\}$

4.3. Temperature distribution

Behavior of dimensionless temperature distribution profile against the perpendicular coordinate y is analyzed graphically for variation values of thermal radiation parameter Rn heat generation parameter B, phase difference parameter $\emptyset$, right wall amplitude ratio parameter a. Figure 8(a) shows an increment behavior on $\theta(y)$ for higher values of Rn toward the left and right walls while hardly effect is seen near the middle part of peristaltic wave for$(-1 \leq y \leq 2)$. Whereas quite opposite features of increasing magnitude of B on $\theta(y)$ is noticed i.e. reduction function depicted near the walls however rise in the profile is observed at the central region of the channel see figuer 8(b). Two different situations in figure 9(a) is concluded for ascending values of $\emptyset$ a decreasing function for $\theta(y)$ at the region $y \in (-4, 1)$ while the feature reversed to an enhancement in for $\theta(y)$ at $y \in (2, 6)$. It can be seen from figure 9(b) that increase value of a reduces the temperature distribution profile.

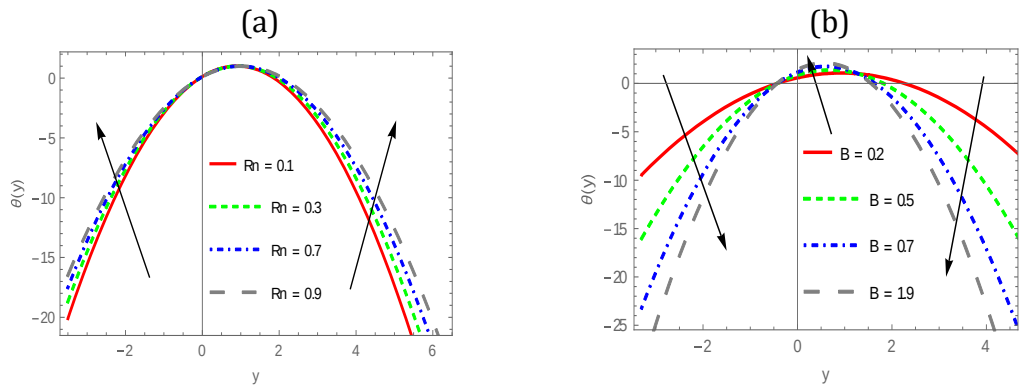

Figure 8: Temperature distribution profile is for different values of (a) thermal radiation parameter Rn (b) heat generation parameter$B$ and when $\{a = 0.1, b = 0.1, d = 0.1, \phi = \frac{\text{Pi}}{6}, x = 0.1\}$

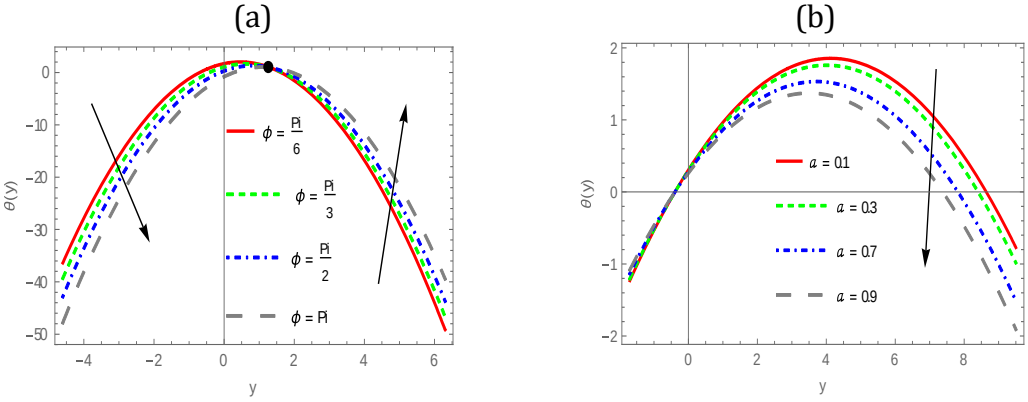

Figure 9: Temperature distribution profile is for different values of (a) phase difference parameter $\emptyset$(b) right wall amplitude parameter a and when $\{b = 0.1, d = 0.1, \text{Rn} = 0.1, B = 0.2, x = 0.1\}$.

4.4. Trapping: stream lines

A phenomenon is another interesting part in our work which defines bolus as a closed amount of fluid trapped by streamlines. We displayed some results of the phenomenon of trapping in figures 10-14. Graphical results show that for ascending values of dimensionless viscosity parameter(ϵ) the trapping bolus shrink in size as shown in figure 10. While figure 11. Highlighted that an increment of Hartman number H due to increases in Lorentz force which resist the fluid flow and as a result the size of trapping bolus decreases. The influences of the porosity parameter on streamlines are shown in figure 12. It shows that rise in porosity parameter κ values tends the trapped bolus to enhance in size and number. From figure 13 we demonstrate that a larger value of phase difference $(\emptyset = \pi)$ diminished the trapped

bolus. We observe that the size and number of the trapped bolus enhance with increasing of Ree-Eyring parameter A shown in figure 14.

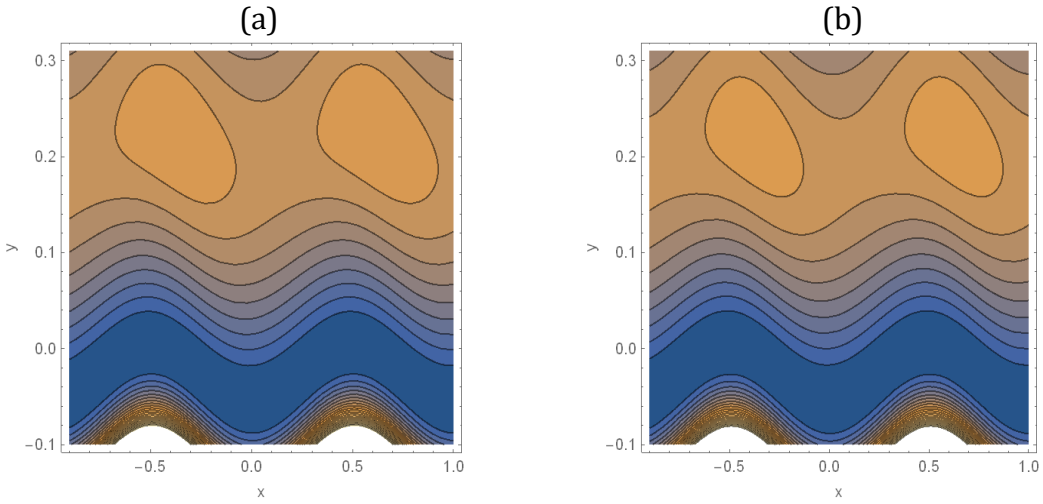

Figure 10: Streamlines is for variation of dimensionless viscosity parameter $\epsilon = \{0.1,0.5\}$ and for fixed parameters $\{a = 0.01, b = 0.1, \mathrm{d}_1 = 0.3, \mathrm{Rn} = 0.3, B = 0.4, \phi = \frac{\mathrm{Pi}}{6}, W = 0.1, H = 0.1, \kappa = 0.1, A = 0.3, \Phi = 0.1\}$

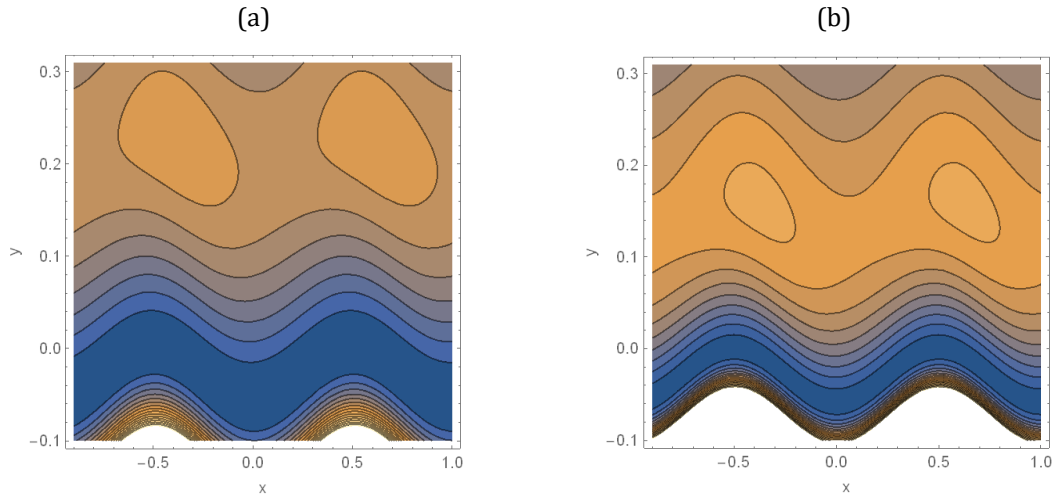

Figure 11: Streamlines is for variation of Hartman number $H = \{0.5,1\}$ and for fixed parameters $\{a = 0.01, b = 0.1, \mathrm{d2} = 0.3, \mathrm{Rn} = 0.3, B = 0.4, \phi = \frac{\mathrm{Pi}}{6}, W = 0.1, \kappa = 0.1, \epsilon = 0.1, A = 0.3, \Phi = 0.1\}$

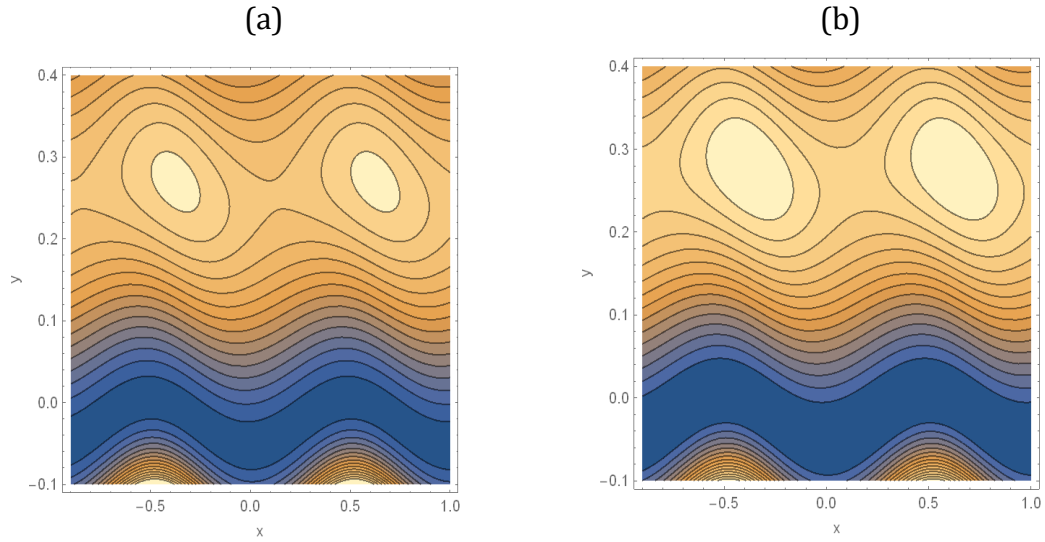

Figure 12: Streamlines is for variation of porosity parameter $\kappa = \{0.5, 2\}$ and for fixed parameters $\{a = 0.01, b = 0.1, \mathrm{d}_2 = 0.3, \mathrm{Rn} = 0.3, B = 0.4, \phi = \frac{\mathrm{Pi}}{6}, W = 0.1, H = 0.1, \epsilon = 0.1, A = 0.3, \Phi = 0.1\}$

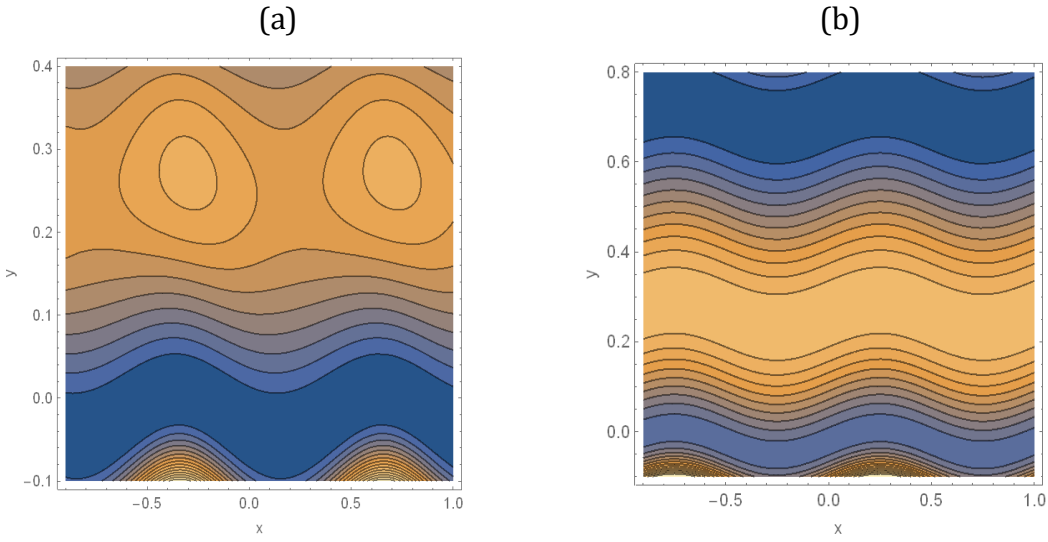

Figure 13: Streamlines is for variation of phase difference parameter $\phi = \{\frac{\pi}{6}, \pi\}$ and for fixed parameters $\{a = 0.01, b = 0.1, \mathrm{d}_2 = 0.3, \mathrm{Rn} = 0.3, B = 0.4, W = 0.1, \kappa = 0.1, \mathrm{H} = 0.1, \epsilon = 0.1, A = 0.3, \Phi = 0.1\}$

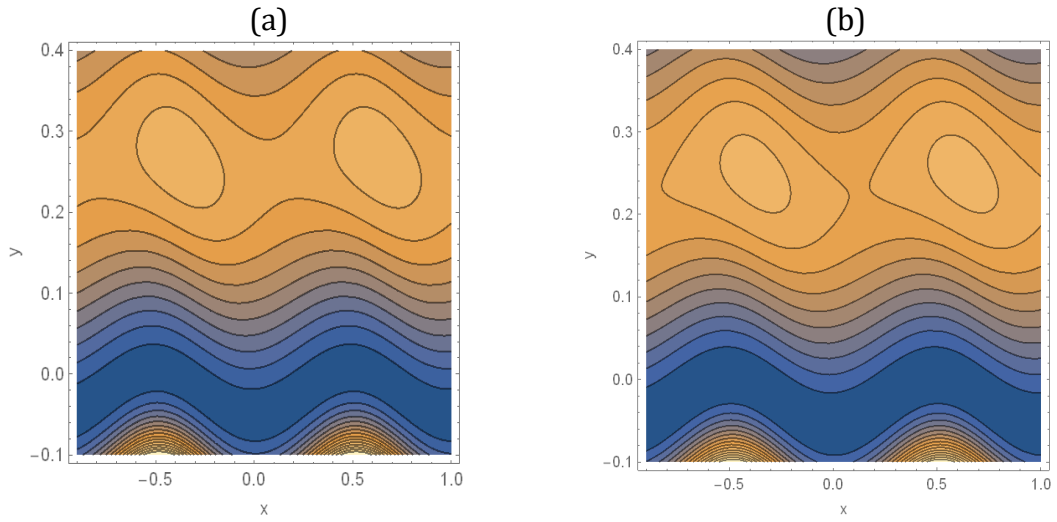

Figure 14: Streamlines is for variation of Ree-Eyring fluid parameter $A = \{0.1, 0.5\}$ and for fixed parameters $\{a = 0.01, b = 0.1, \mathrm{d2} = 0.3, \mathrm{Rn} = 0.3, B = 0.4, \phi = \frac{\mathrm{Pi}}{6}, W = 0.1, H = 0.1, \kappa = 0.1, \mathrm{Gr} = 0.1, \epsilon = 0.1\}$

5. Conclusion

The peristaltic transport of non- Newtonian (MHD) blood flow Ree-Eyring fluid with temperature-dependent viscosity influence through a porous medium flows in an asymmetric channel is studied. Considering assumptions of long wavelength and low Reynolds number the problem are simplified and reduced into a set of nonlinear differential equations in which the equations of temperature distributions is solved analytically, while for finding the stream function we employed a perturbation method. A parametric analysis is permitted through various graphs that made us found conclusions with some important perceptions

1. The velocity profile attained a parabolic structure as well as its magnitude remains stable in the central part of the channel for all parameters. Moreover, we noticed from figures that the velocity axial reduces due to increases in Hartman number H whereas opposite behavior for porosity parameter κ.

2. The two Ree-Eyring parameters A and W have an opposite effect on velocity axial. However, the velocity profile enhances along the left wall while, inverse relationship is seen toward the right wall for higher values of dimensionless viscosity parameter ϵ.

3. The temperature distribution is an increasing function near the walls and reduction function in the middle region from the channel with the thermal radiation parameter Rn, but the feature is reversed for increment magnitude of heat generation parameter B.

4. Rise in H and Ree-Eyring W parameters caused deceleration in the axial pressure gradient near the walls and increases at the central part of the channel. While, the behavior is reflected for high values of phase difference parameter ϕ, and porosity κ.

5. The impact of ϵ and κ on pressure rise are qualitatively similar. They enhance the pumping region and retard the augment pumping region while the impact of H and W parameters on pressure rise are quite opposite.

6. It is predicted that the trapped bolus disappeared when the phase difference parameter is $(\phi = \pi)$. Furthermore, larger value of A parameter increases the trapped bolus in size and number.

References

[1] Abbasi. F. M, Hayat. T and Ahmad. B, Hydro magnetic Peristaltic Transport of Variable Viscosity Fluid with Heat Transfer and Porous Medium, Appl. Math. Inf. Sci., (2016), 10(6), 2173-2181.

[2] Akbar. N. S, Non- Newtonian Model Study for Blood Flow through a Tapered Artery with a Stenosis. Alex. Eng., (2016), J, 55, 321-329.

[3] Abdul Wahab Hafiz, Zeb Hussan, Bhatti Saira, Gulistan Muhammad, Kadry Seifedine and Nam Yunyoung, Numerical Study for the Effects of Temperature Dependent Viscosity Flow of Non-Newtonian Fluid with Double Stratification. Appl. Sci. 2020, 10, 708.

[4] Bhatti. M. M, Ali Abbas. M and Rashidi. M. M, Combine effects of Magneto hydro dynamics (MHD) and partial slip on peristaltic Blood flow of Ree–Eyring fluid with wall properties. Engineering Science and Technology, an International Journal, (2016), 19, 1497–1502.

[5] Bhatti. M. M and Rashidi. M. M, Study of heat and mass transfer with Joule heating on magneto hydro dynamic (MHD) peristaltic blood flow under the influence of Hall Effect. Propulsion and Power Research, (2017), 6(3):177–185.

[6] Ellahi. R, Bhatti. M.M and Vafai. K, Effects of Heat and Mass Transfer on Peristaltic Flow in a non- Uniform Rectangular Duct, International Journal of Heat and Mass Transfer, (2014), 71, 706-719.

[7] Goud. B. Shankar, Babu. B. Suresh, Shekar. MN Raja and Srinivas.G, Mass Transfer Effects on MHD Flow through Porous Medium past an Exponentially Accelerated Inclined Plate with Variable Temperature and Thermal Radiation, International Journal of Thermo fluid Science and Technology (2019), Vol. 6, No. 4, Paper No. 19060402.

[8] Hussain Azad, Akbar Sobia, Sarwar Lubna, Nadeem Sohail and Iqbal Zaffar, Effect of time dependent viscosity and radiation efficacy on a non-Newtonian fluid flow, Heliyon 5 (2019) e01203.

[9] Kumar Gaurva, Kumar Atul, Mirsa Manoj Kumar and Srivastava Vibhawari, Chimecal Reaction Effect on MHD flow past an impulsively started started vertical cylinder with variable temperature and mass diffusion, Journal of Science and Arts, (2019),
2(47), pp. 513-522.

[10] Kumar. S. R, Analysis of Heat Transfer on MHD Peristaltic Blood Flow with Porous Medium through Coaxial Vertical Tapered a symmetric Channel with Radiation-Blood Flow Study, Int.J. Bio-Science & Bio-Tech, (2016), 8(2), 395-408.

[11] Mallick. B, Sinha. A and Misra. J. C, Heat and Mass Transfer in A Symmetric Channels During Peristaltic Transport of an MHD Fluid Having Temperature-Dependent Properties, Alex. Eng. J. ., (2016).

[12] Misra. J. C and Maiti. S, Peristaltic Pumping of Blood through Small Vessels of Varying Cross-Section", Journal of Applied Mechanics, (2012), 79(6), 061003 (19 pages).

[13] Misra. J. C, Mallick. B and Sinha A, Heat and Mass transfer in A Symmetric Channels During Peristaltic Transport of An MHD Fluid Having Temperature-Dependent Properties", Alex. Eng. J, (2016), 55(2), 1225-1234.

[14] Ramesh. K and Devakar M, Effect of Heat Transfer on The Peristaltic Transport of a MHD Second Grade Fluid Through A Porous Medium In An Inclined Asymmetric Channel, Chinese Journal of Physics,55(3), (2017), 825-844.

[15] Riaz, A, Nadeem. S and Ellahi. R, Effects of The Wall Properties on Unsteady Peristaltic Flow of An Eyring- Powell Fluid in A Three-Dimensional Rectangular Duct, (2015), 8 (6), 1550081 (17 pages).

[16] Reddy. M. G, Reddy. k. V and Makinde. O .D, Heat Transfer on MHD Peristaltic Rotating Flow of Jeffery Fluid in an Asymmetric Channel, Int. Appl. Comput. Math, DoI, (2016), 10. 1007/s40819-016-0293-1.

[17] Sunitha,G and Asha,S.K, Effect of joule heating and MHD on peristaltic blood flow of Eyring–Powell nanofluid in a nonuniform channel, Journal of Taibah University for Science, (2019), 13:1, 155-168.

[18] Veerakrishna. M and Swarnalathamma. B. V, Convective Heat and Mass Transfer on MHD Peristaltic Flow of Williamson Fluid with the Effect of Inclined Magnetic Field, AIP. Conf. Proc., (2015), 1728, 020461-1-020461-8(pages).